AIMS Materials Science, 4(1): 102-117.
DOI: 10.3934/matersci.2017.1.102
Received: 08 November 2016
Accepted: 27 December 2016
Published: 05 January 2017

http://www.aimspress.com/journal/Materials

Research article

Deformation mechanism of kink-step distorted coherent twin boundaries in copper nanowire

Bobin Xing [1], Shaohua Yan [1], Wugui Jiang [2], and Qing H. Qin [1,*]

[1] Research School of Engineering, Australian National University, Acton, ACT 2601, Australia
[2] School of Aeronautical Manufacturing Engineering, Nanchang Hangkong University, Nanchang 330063, China

* **Correspondence:** Email: Qinghua.Qin@anu.edu.au; Tel: +61-0261258274; Fax: +61-0261255476.

Abstract: In the construction of nanotwinned (NT) copper, inherent kink-like steps are formed on growth twin boundaries (TBs). Such imperfections in TBs play a crucial role in the yielding mechanism and plastic deformation of NT copper. Here, we used the molecular dynamic (MD) method to examine the influence of kink-step characteristics in depth, including kink density and kink-step height, on mechanical behavior of copper nanowire (NW) in uniaxial tension. The results showed that the kink-step, a stress-concentrated region, is preferential in nucleating and emitting stress-induced partial dislocations. Mixed dislocation of hard mode I and II and hard mode II dislocation were nucleated from kink-step and surface atoms, respectively. Kink-step height and kink density substantially affected the yielding mechanism and plastic behavior, with the yielding stress functional-related to kink-step height. However, intense kink density (1 kink per 4.4 nm) encourages dislocation nucleation at kink-steps without any significant decline in tensile stress. Defective nanowires with low kink-step height or high kink density offered minimal resistance to kink migration, which has been identified as one of the primary mechanisms of plastic deformation. Defective NWs with refined TB spacing were also studied. A strain-hardening effect due to the refined TB spacing and dislocation pinning was observed for defective NWs. This study has implications for designing NT copper to obtain optimum mechanical performance.

Keywords: molecular dynamic simulation; nanotwins; dislocations; defective twins

1. Introduction

Nanotwinning is believed to be a feasible strategy for improving the strength and ductility of metals. Nanotwin lamellae found in metals can be categorized into three main groups: growth twins, deformation twins, and annealing twins [1–4]. Growth twins are extensively fabricated via electrodeposition or magnetron sputtering, and two types of TBs are usually observed in growth twins, namely coherent twin boundaries (CTB) and incoherent twin boundaries (ITB). Despite the density of CTBs outweighing that of ITBs, they both play important roles in affecting mechanical behavior in NT metals [5].

Extensive studies have focused on the mechanical performance of CTB-dominated nanotwinned structures [6–10]. Strengthening phenomena have been observed in several experiments and MD work [11–14], in which grain refinement led to a significant improvement in peak stress before the nucleation event. It is well-established that the presence of CTBs that obstruct the transmission of dislocation often favors a substantial increase in strength. Moreover, yield strength is inversely proportional to CTB spacing (denoted by λ), where a decrease in λ increases the likelihood of interaction of CTB and dislocations. At this stage, the mechanisms of TB-strengthening phenomenon are tentatively understood via existing experiments and simulations. After all, most of the twin lamellae used for MD modeling were assumed to be defect-free, based on in-situ observations of CTBs. Thus, yield stress can be approximated as the stress required for nucleation of the first dislocation and the yielding mechanism is attributed to Schmid factor analysis based on the loading direction.

To the best of the authors' knowledge, there are few studies of defective NT metals or TBs with kink-like steps. The presence of kink-steps tends to trigger multiple slip systems and tailor mechanical performance. This type of defective TB has been identified using high-resolution inverse pole figure orientation mapping (IPFOM) [15], the converse of a perfectly flat TB. The density of kink-steps was suggested to be an average of one kink per 10-nm length, which is within the scale of current MD simulation. The kink-step can be represented by ITB segments, in which the movement of a kink-step corresponds to detwinning [16,17]. The influence of interaction between kink-step and screw dislocation on hardening and ductility is well-investigated [18]. Those investigations greatly shape our understanding of TBs and deformation mechanisms. Kink migration, a softening behavior, is believed to be the dominant mechanism when a TB is stretched in the twin growth direction [15]. The motion of the ITBs facilitates the achievement of better ductility in the NW and a decrease in yield strength. Investigations on ITB/CTB junctions in bicrystal models were carried out by researchers [19,20]. The ITB migration was caused by external deformation or thermally driven force, where the impact of dislocation interaction was rarely discussed. And the migration mechanism was found to closely relate to shear stress exerted on ITBs. However, insufficient atomistic investigation was performed to explore the significance of the propensity of kink-steps in NT NWs, in which the presence of TB strengthens the NW. In particular, some questions remain with regard to the yielding mechanism and the plastic mechanism of defective NT copper NW: Does the presence of a kink-step always weaken the material? Is high kink density beneficial to mechanical behavior? How does kink-step migrate with the presence of dislocations? Does the defective NW with kink-steps strengthen by virtue of confined TB spacing (λ)?

To answer the questions cited above, we present a molecular dynamic simulation study to access the influence of kink-steps on the mechanical behavior of parallel-twinned defective NWs. We

first compare the mechanical behavior of NWs with perfect TBs and with defective TBs with different kink-step density. Then, the influence of kink height on yielding mechanism and plasticity is discussed. The mechanism for kink migration is discussed. Lastly, the mechanical behaviors of defective NWs with different values of TB spacing are compared, focusing on details of TB-mediated strain hardening and dislocation pinning.

2. Molecular Simulation

The MD simulations in this work were performed using LAMMPS [21]. The embedded-atom-potential developed by Mishin [22] was utilized to describe the interplay among the Cu atoms, because the potential accurately predicts stacking faults and twin formation energies. The spurious influence of fixed ends in the axial direction was eliminated by imposing periodic boundary conditions. In contrast, free boundaries were applied to the sidewalls to simulate a nanowire. The $[11\bar{2}]$ direction was arranged along the length dimension, while the TB planes were allocated in the [111] and $[1\bar{1}0]$ lateral plane, implying y axis and z axis, respectively. The twin plane was set parallel to the NW axis in the whole work, sitting in the very middle of the NW. That arrangement allowed stabilization of the kink-step throughout the relaxation. All tested specimens were $36 \times 8 \times 8$ nm^3 in size. The kink-steps were added on the TBs by introducing a displacement field in the (111) direction. The displacement field was varied from 0 nm (perfect) to 1.8 nm (nine-atom-layer kink). To investigate the effect of kink density on defective NWs, four distinct kink-step densities, namely 20, 10, 8 and 5 $[11\bar{2}]$ lattice spacings, were created simultaneously, which are equivalent to 17.7 nm, 8.8 nm, 7 nm and 4.4 nm. After relaxation, the resultant kink-steps were found to be similar to the structural units in ITBs, a finding that was consistent with previous studies [15]. Furthermore, to highlight the influence of additional twin plane, defective NWs attained twin spacing of 3.1 nm and 1.8 nm were created, with kink height of two [111] lattice spacing and kink density of 1kink/17.7nm unchanged.

Prior to the equilibrium process, molecular static simulations were employed using the conjugate gradient method. Each configuration was then equilibrated to a temperature of 1 K and zero pressure in the loading direction for 20 ps under an isothermal-isobaric ensemble with a Nose-Hoover thermostat. The time-step was set as 2 fs. The equilibrated specimen was then deformed in tension along the length direction at a strain rate of 10^8 s^{-1}, with the environmental temperature controlled at 1 K under canonical ensemble (NVT). High strain rate in MD was found to induce amorphous deformation [23] and low strain rate in MD is computational demanding. The low temperature allowed exploration of the incipient plasticity mechanism of the system without any thermal impact. Virial theorem was implemented to yield the stress within the NWs, and the tensile stress was defined by the average of all atomistic stresses. Deformation potential energy is calculated by the difference between initial potential energy after relaxation and potential energy during deformation.

To discern the preferable defects activated in the progress of deformation, the visualization tool Ovito was utilized [24]. It analyzes the generated atomic-level configurations and identifies dislocation activities using the common neighbor analysis (CNA) [25]. The perfect FCC Cu atoms are colored in green, while the HCP atoms are colored in red. Other atoms are grey. Partial dislocation <112>-{111} is indicated by the other atoms colored grey. A twin boundary is represented by a single layer of hexagonal close packing (HCP) atoms, while an intrinsic stacking

fault is plotted by two adjacent layers of HCP atoms.

3. Results

In presenting the results, the stress-strain curve and deformation potential energy of perfectly twinned NWs and defectively twinned NWs with different number of kink-steps are first compared. The existence of kink-steps introduces distinct slip systems from those of perfect NWs. Then, the influence of kink-step height and twin spacing are investigated. Simulation models used in the sections are presented in supplementary materials.

3.1. Mechanical performance of perfectly and defectively twinned NWs

3.1.1. Strain-stress curves and deformation potential energy

We firstly take a close look at the evolution of mechanical performance with and without the presence of kink-steps. In this subsection, the kink-step height was kept fixed at 1.2 nm by displacing TB plane in [111] direction. Different kink densities were introduced, namely 17.7 nm, 8.8 nm, 7.0 nm and 4.4 nm, which accommodate one to four kink segments in the length direction. Whereas the kink-step density in the existing study was found to be one kink per 10 nm along the CTB [15]. Figure 1 (a) compares the engineering strain-stress curves between a perfectly twinned NW (perfect NW) and defectively twinned NWs (defective NWs). In the perfect NW, we can see that (1) a precipitous drop occurs after the initial yielding point; (2) the NW with perfect CTB displays nearly twice the tensile stress compared to those of the defective NWs. On the other hand, there is a clear trend of a decrease in peak stress with the transition from one kink per 17.7-nm-long NW to 7-nm-long NW. That trend, however, does not extend to the one kink per 4.4-nm-long NW. The peak strength obtained by the 4.4 nm-kink-density NW nearly approximates to that of the one kink per 17.7 nm NW. Moreover, the insert in Figure 1 (a) shows a series of minor dislocation activities before the precipitous drop in stress. Six consecutive cusps are found, corresponding to the same number of partial dislocation events, revealed in Figure 1 (c). The first partial dislocation takes place at the applied strain of 4.0% from the kink-step denoted as (1) in the insert in the Figure 1 (a). That dislocation nucleation does not account for any decline in stress and deformation energy. It further strengthens the NW until multiple dislocation events activate in sequence from an array of kink-steps.

Figure 1(b) further demonstrates the accumulation of deformation potential energy of perfect and defective NWs in the course of tension. It is evident that the difference in critical deformation potential energy determines the elastic deformation period and the yield stress. In the figure, both perfect and defective NWs accumulate potential energy in the same pattern at the beginning of the deformation. The presence of ITB segments in the defective NWs results in an earlier yield point In contrast, the NWs with perfect TB remain in a defect-starved state until the applied strain reaches 8.5%. In addition, an increase in the number of kink-steps leads to a reduction in critical deformation potential energy. However, the NW with confined kink density does not sustain a low critical deformation potential energy, due to the consecutive dislocation activities in the kink-step regions.

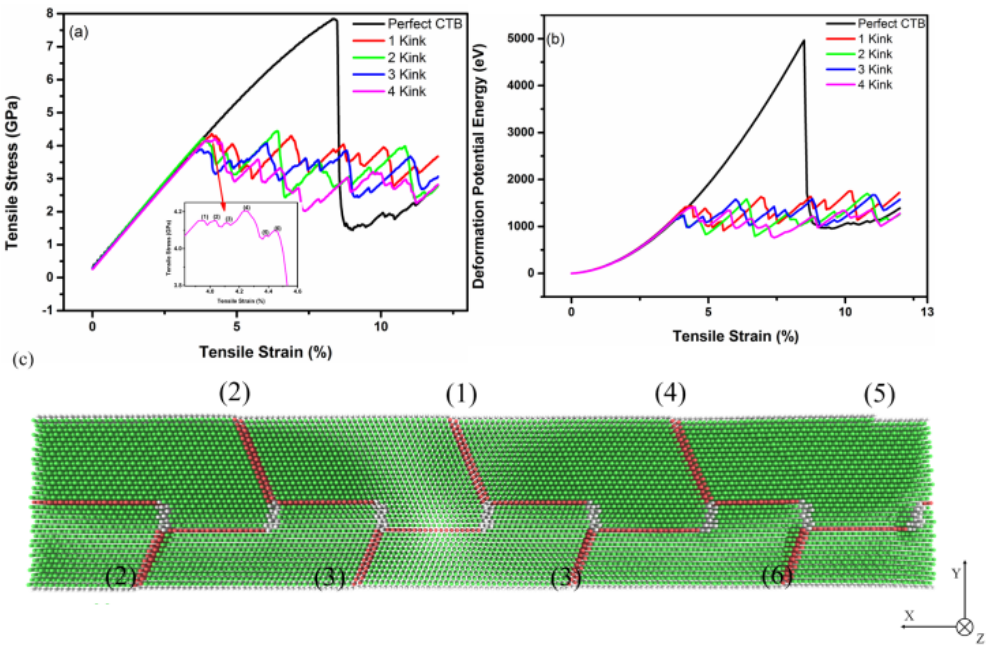

Figure 1. Effect of kink-step density on mechanical behaviour of parallel-twinned Cu NWs computed. (a) Stress-strain curve. (b) Deformation potential energy. (c) The sequence of dislocation nucleation prior to stress drop for 4.4 nm-kink-density NW.

3.1.2. Nucleation of dislocations and plastic deformation

In Figure 2, the atomic configurations of the first dislocation nucleation of perfect NW and defective NWs are compared. In Figure 2 (a), two segments of CTB are separated by the six (111) layered ITB, which represents a kink-step in this work. The twin and matrix lamellae are mirror symmetrical in crystal orientation due to the presence of the TB, leading to a discontinuity of slip systems. The kink-step is represented by an array of edge partial dislocations b1 ($\frac{1}{6}[1\ 1\ \bar{2}]$) and mixed partial dislocation b_2 ($\frac{1}{6}[\bar{2}\ 1\ 1]$) and b_3 ($\frac{1}{6}[1\ \bar{2}\ 1]$), respectively [26]. In longitudinal loading, the Schmid factor (0.39) for leading partials in the preferred slip system outweighs that of trailing partials (0.31). At the yield point, the leading partials tend to nucleate and glide, without the presence of trailing partials. From Figure 2 (b) and (c), the preferred sites of the first dislocation nucleation vary depending on TB conditions. The ITB segments of the defective NW serve as the sources for nucleation, while the surface atoms are the primary source of nucleation for the perfect CTB. Two distinct slip systems are activated from the defective Cu and perfect Cu, respectively, similar to existing investigation on the yielding mechanism [27,28]. The models of dislocations are referred to as "hard mode I" and "hard mode II", shown in Figure 2 (d) and (e). Hard mode I dislocations are favoured when tension/compression normal to the TB is applied, due to high Schmid factor. Both the slip direction and the slip plane are inclined to the TB. When loading direction is parallel to TB plane, hard mode II dislocations will glide on the slip plane inclined to TB and travel in the direction parallel to (111) plane.

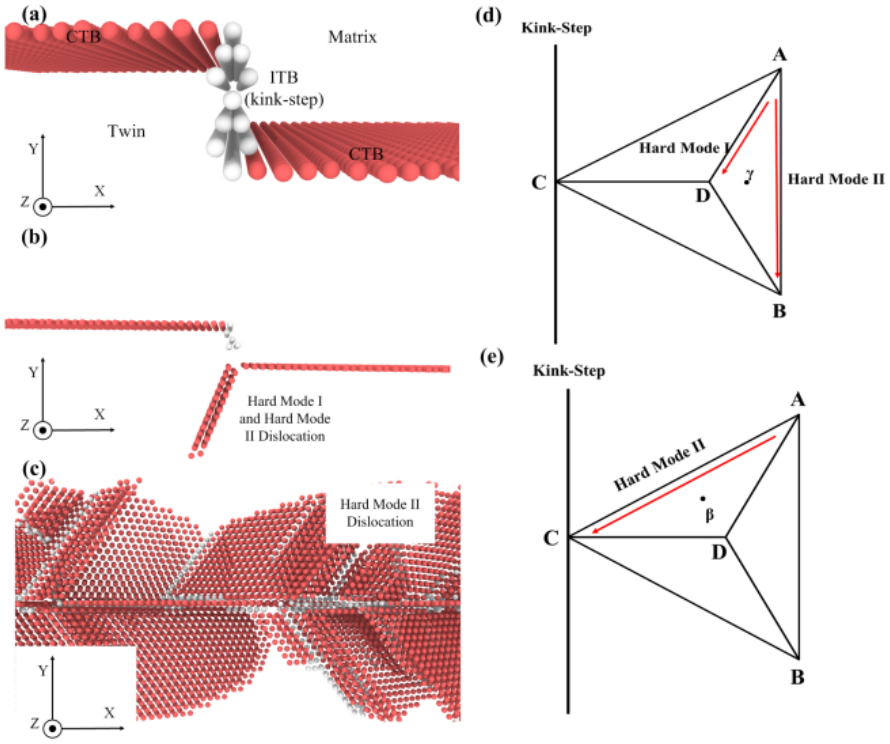

Figure 2. Atomic configurations of the local crystal structure of parallel-twinned Cu NWs at the yielding point. (a) Illustration of kink-step structure. (b) Defective NW with 1 kink at ε = 4.0%. (c) Perfect NW at ε = 8.5%. (d) Mixed mode dislocation from kink-step on Thompson tetrahedron. (e) Hard Mode II dislocation in Thompson tetrahedron.

Hard mode I dislocation can coexist with hard mode II dislocation via nucleating from slender TB (kink-steps), which promotes of dislocation-TB interaction, in turn tuning mechanical performance. The dislocation from kink-steps does not give rise to symmetrical dislocation nucleation in both twin and matrix grains. In contrast to the defective NW, multiple partial dislocation bursts are seen from the external surfaces in the perfectly twinned NW at a relatively high strain. Since twin and matrix contain the mirror symmetric crystallographic orientation and same maximum Schmid factor [27], the slip systems are activated simultaneously on the two sides of the TB and no secondary slip plane can be seen. Leading partials nucleate and emit from the surface atoms and interact with TB atoms with further straining. The movies of the NW with 1 kink/17.7 nm and 1 kink/4.4 nm are recorded in the supplementary material: movie 1 and 2.

In existing works, two possible reactions may occur when such a hard mode II dislocation encounters a TB on its slip plane, namely the generation of a stair-rod joint or a cross-slip [12,27]. Stair-rod ($\delta\beta$) dislocations indicated in Figure 3 demonstrate dislocation-TB interaction via:

$$C\beta \rightarrow C\delta + \delta\beta \tag{1}$$

Stair-rod dislocations could further dissociate into two partial dislocations δC and $C\beta$ by overcoming higher energy barrier [29], causing migration of TB and one-atom layer transmission in TB. Alternatively, hard mode II dislocations like *AB, AC* and *BC* can slip both in the matrix and the twin. Transmission of partial dislocation across twin boundary is also achieved via:

$$A\alpha \rightarrow A\alpha' + \alpha'\alpha \quad (2)$$

$A\alpha'$ is the partial dislocation slips in the twin and $\alpha'\alpha$ is the sessile stair-rod dislocation formed by invoking double Thompson tetrahedron [29], as shown in Figure 3.

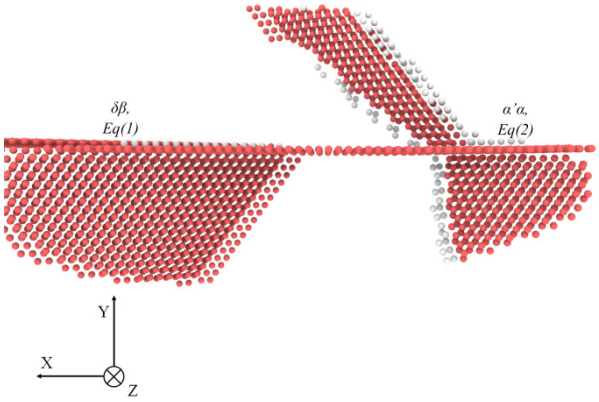

Figure 3. TB-partial dislocation interaction within defective NWs at ε = 5.1%.

Furthermore, a large kink density introduces marked TB activity in the course of the deformation. Unlike the low-kink-density NWs, twin partial multiplication and kink-step migration are more likely to occur during the plastic deformation as shown in Figure 8, where two representative snapshots are presented at 5.0% and 11.5% of ε, respectively. The motion of a kink in pure tension is seen clearly at the places marked "M". This phenomenon was previously covered in defective GB models, where a tension parallel to the CTB was imposed [15]. The initial ITB segments are dissociated due to the partial dislocation nucleated at kink-steps, and the kink-steps are then divided into a few one-layer micro-kink-steps. The tension parallel to the TB gives a rise to kink migration, where the critical shear strength is much lower than that of NWs deformed in the (111) direction (~10 GPa) [9]. Other TB migrations are accomplished via the reaction by overcoming excessive energy barrier:

$$\delta\beta \rightarrow \delta A + A\beta \quad (3)$$

Stair-rod dislocation ($\delta\beta$) formed during the interplay of partial dislocation and twin boundary dissociates with increased stress concentration, resulting in the migration of TB. In addition, at the location marked "TP", additional twinning partials are formed. The marked region consists of the original TB layer and a twinning partial, as shown in the insert in Figure 4. The twinning partial ($\frac{1}{6}[1\ 1\ \bar{2}]$) that slips on the twin plane is found to emit from the kink-steps. Due to unfavourable Schmid factor, it cannot be nucleated at the initial yielding point. Twinning partial only nucleates with sufficient stress concentration, and is short-lived and destroyed with increased strain. At ε = 11.5%, kink migration is found, with some kink-steps shifting horizontally and other kinks merging into one kink-step. The leftmost one-layer step travels a large distance between two snapshots. This finding leads to the implication that the height of a kink-step determines the kink migration velocity. A short kink-step gives a rise to kink migration, thereby leading to detwinning in the NW. Previously generated twin layers disappear at the kink-step and the initial 1.2 nm-height kink-step is also

reduced to a one-layered kink-step. This is due to the interaction of dislocation-TB, which keeps the TB climbing vertically. Such activities undermine the role of the kink-step in plastic deformation. Fewer kinks create dislocation embryos and the flow stress is substantially lower than other NWs with different kink density.

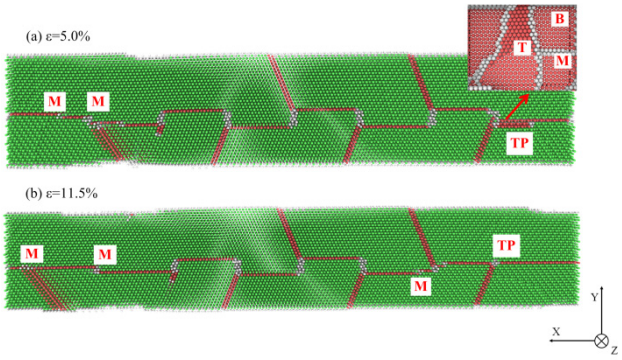

Figure 4. Microstructures in the NW with 4.4-nm kink density at different stages of tension. M represents kink migration, TP represents twin multiplication. Insert: [111] view of the TB layers at ε = 5.0% with perfect Cu atoms removed. T: top layer, M: middle layer, B: bottom layer.

3.2. Effect of kink height

Besides the number of kink-steps, another notable characteristic of defective NW is the height of the kink-step. From existing works on the deformation of TBs, we understand that twinning partial multiplication occurs where an incident dislocation approaches the CTB plane and a few layered steps are formed. That conclusion has been verified via experiments and numerical simulation [15,30]. Depending on the parameters used in the fabrication of growth twins, it is feasible that the growth twin is comprised of different heights of kink-steps. IPFOM reveals that the typical step height ranges from ~1 to 5 nm [15]. In this work, a kink-step is constructed by shifting a sector of a CTB in the [111] direction. To ensure completeness of the kink-step (an array of ITB segments), the vertical displacement needs to be an integral number of (111) plane spacing. Four levels of kink-step height were utilized to investigate the influence on mechanical behaviour in NT Cu, namely 0 nm (perfect TB), 0.6 nm (three atom layers), 1.2 nm (six atom layers) and 1.8 nm (nine atom layers). Four specimens were deformed in the (112) direction with a strain rate of 10^8 s^{-1} at 1 K.

Figure 5 depicts the variation in tensile strength and deformation potential energy in relation to kink-step height. A prediction is made that the peak strength is inversely proportional to the kink height. NWs with smaller kink height or perfect NWs are unlike to readily yield since the ITB segments are the predominant source of nucleation. On the other hand, the presence of excessive ITB segments may result in augmented localized stress, suggestive of the introduction of a shear band in these highly defective samples. The simulated stress-strain curve shows that the peak strengths decline from the 0-nm-kink-height NW to the 1.8-nm-kink-height NW, a result that is in good agreement with the prediction. A strain-hardening phenomenon is noticed in the 1.8nm-kink-height NW where an incident partial dislocation generates from the kink-steps at the strain of 3.4%, as schemed in Figure 4 (c). This dislocation event accounts for a minor drop in the tensile strength and

in the deformation potential energy, converse to NWs with shorter kink height. The accumulation of deformation energy remains uninterrupted until a dislocation burst occurs in Figure 4 (d). The process of deformation in 0.6-nm-kink and 1.8-nm-kink are recorded in supplementary movies 3 and 4.

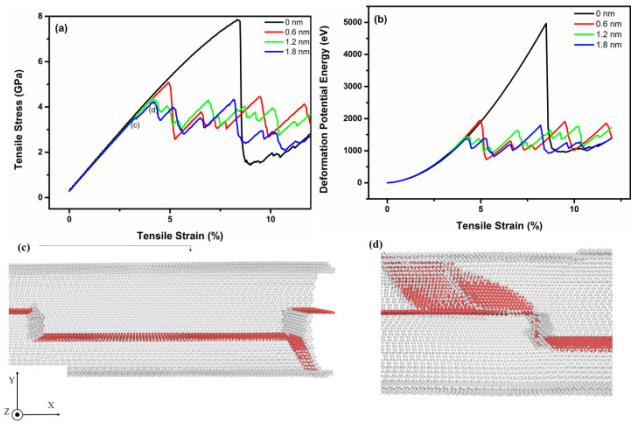

Figure 5. Effect of kink-step height on mechanical behaviour of parallel-twinned Cu NWs computed. (a) Stress-strain curve. (b) Deformation potential energy. (c) Initial yield point of 1.8nm-kink-height NW at ε = 3.4%. (d) Dislocation burst of 1.8nm-kink-height NW at ε = 4.3%.

3.3. Twin-spacing-dependent deformation mechanism

In the preceding sections, each NW contained only one TB plane; in other words, sufficiently TB spacing (λ) was allocated for the samples. TB spacing has been recognized as the predominant characteristic in strengthening ultrahigh-twin-density NT metals. Extensive studies have disclosed that NT strength is inversely proportional to TB spacing, suggesting that dislocation activities are impeded by the confined twin spacing. Nevertheless, this finding is dependent on the loading direction. NT Cu with confined perfect TB does not show an ascending trend in yield strength, as the dislocation nucleation is not impeded by the TB [27]. Here we construct NT Cu of defective TB and perfect TB with different λ ranging from 1.8 nm to 4 nm, while kink-height was fixed at six layers of (111) planes. Selected defective specimens are relaxed and deform in the same manner as the NWs in the previous section.

Figure 6 (a) shows the variation of yield strength and peak strength of perfect and defective NWs with different TB spacings. In the perfect NWs, the confined TB spacing contributes to a small improvement in strength and ductility. Slightly higher peak stress is found with increase of twin boundary spacing, suggesting that more deformation potential energy is required. When the TB is parallel to the loading direction, strengthening effect from TB seems to be minor, as hard mode II dislocation readily transmits across the TB instead of pile-up at TB region for hard mode I dislocation. On the other hand, the defective NW with larger twin density yields at a substantial low strength. The stresses of defective NWs grow in the same manner in elastic deformation until reaching an early yield point. The peak strength of NWs with kink-steps is inversely proportional to the spacing (λ). Notably, the defective NWs with 1.8nm-spacing and 3.1 nm-spacing display a

strain-hardening phenomenon after the yield point. A strengthening effect is introduced by the additional layer of defective TB. High local stress state in kink-steps region nucleate dislocation in ABD plane; however, instead of impeded after traveling for a period in the matrix in 4.0 nm-spacing NWs, the nucleated dislocations in multi-TB NWs are found to be impeded by the surrounding kink-steps or surface, shown in Figure 7. Confined twin spacing not only leads to a smaller yield strength but also introduces much shorter traveling distance for dislocation before they are constrained. We speculate this pinning effect could account for strengthening.

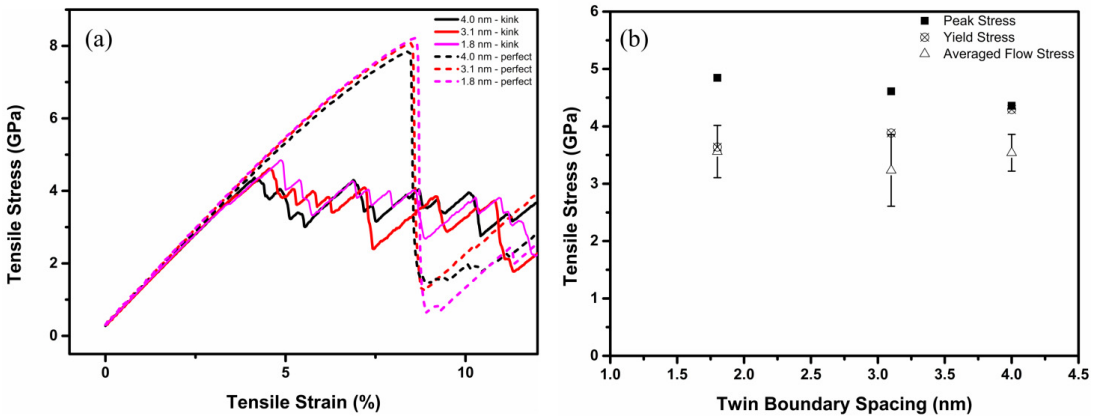

Figure 6. Effect of TB spacing (λ) on (a). stress-strain curves of parallel-twinned Cu NWs. (b) peak stress, yield stress and averaged flow stress from ε = 5% to 12%, with standard deviation bar.

In addition, averaged flow stress against twin boundary spacing is schemed in Figure 6 (b) [31]. No obvious twin-spacing related strengthening or weakening effect on flow stress is spotted.

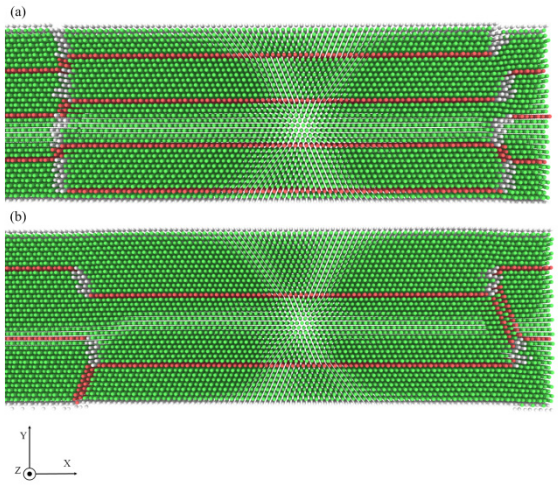

Figure 7. Dislocation pinning in NWs of small twin-boundary spacing. (a) 1.8 nm. (b) 3.1 nm.

In this subsection, we concentrate on how confined TB spacing influences the mechanical behaviour of NT Cu. In previous studies, many researchers have found that loading in the TB growth

direction does not affect the yield strength of perfect NW. From our simulation, however, we show a slight increase in peak strength for defective NW. This phenomenon owes much to the dislocations on ABD plane nucleated from this defective NW, where are usually nucleated under deformation perpendicular to the TB plane. Therefore, we believe that the presence of kink-step tunes the mechanical performance corresponding to the TB spacing.

4. Discussion

4.1. Kink migration mechanism with varied kink-height

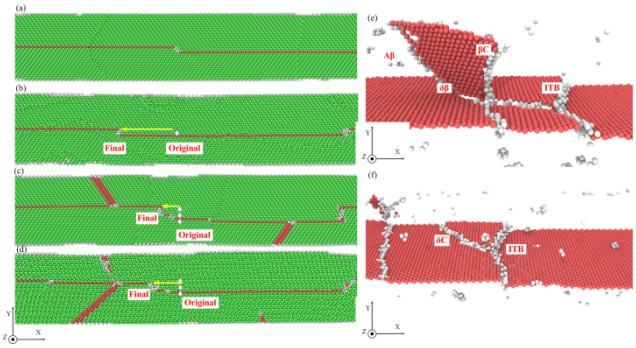

Figure 8. Kink migration in NWs at ε = 12%. (a-b) microstructure of 0.6-nm-kink-height NW at 1 K and 300 K. (c-d) microstructure of 1.8-nm-kink-height NW at 1K and 300 K. (e-f) kink migration mechanism of 0.6-nm-kink-height NW at 300 K. Yellow arrows indicate kink migration distance.

From the previous study on different height of ITB/CTB, significant migration velocity difference was spotted at room temperature. This difference is strong functional-related to kink-height. Migration of ITB junction has been activated by either thermodynamic driving force or shear force τ [26,32]. For instance, ITB comprises three partial dislocations, the resolved glide force acted on a dislocation (Peach-Koehler force) is described via [33]:

$$F=-\tau_{yx}b+F_{interaction}+\gamma_{SF}+F_P \quad (4)$$

The first term describes the impact of the applied shear stress; the second term highlights the dislocation interaction force; the third term represents the tension produced by the stacking fault energy associated with the partial dislocation b. The last term describes the Peierls forces. The Peierls force is found to closely relate to the kink height, as a short kink-step withstands much less frictional force. In other words, short kink is supposed to migrate due to exerted shear force. However, in this study, limited TB migration is spotted even for the one unit ITB. We believe such phenomenon is attributed to low simulation temperature (1 K) used. To reveal the potential dependence of kink migration on temperature, we carried out another MD simulation of the NW with 0.6-nm-kink height and 1.8-nm-kink height at 300 K. The videos of kink migration of distinct kink heights at 300 K are provided in the supplementary material. The video are recorded from ε = 2% to 12%.

In Figure 8 (a) and (b), a significant gap in migration distance is identified using the yellow arrows at two temperatures. The kink-step at 300 K readily shifts horizontally while the kink-step at 1 K travels limited distance. In Figure 8 (c) and (d), at both 1 K and 300 K, noticeable kink disassociations are found at the kink-steps, suggestive of the interaction of dislocation and kink-step that caused movement of kink-step. The migration of complete ITB segment is demanding when kink height is large, whereas migration distance of single ITB segment is readily achieved. However, existing studies have not included dislocation-kink interaction as the dominant mechanism for the kink-migration. Due to the constraints in boundary condition and the geometry of the NW, more dislocation-kink interactions are found. Thus, we conclude that the migration of the kink-step results from the reaction with dislocations, as shown schematically in Figure 8 (e) and (f). The initial reaction is completed by:

$$A\beta \rightarrow A\delta + \delta\beta \tag{5}$$

Leading partial $A\beta$ reacts with CTB, leaving stair-rod dislocation $\delta\beta$ on the CTB and (111) TB layer climb. Then, the trailing dislocation further reacts with sessile stair-rod dislocation to form a (111) plane partial dislocation.

$$\delta\beta + \beta C \rightarrow \delta C \tag{6}$$

ITB, the ensemble of partial dislocation $A\delta$, $B\delta$ *and* $C\delta$, will start migration towards dislocation transmission direction in a short period.

4.2. Influence of dislocation pinning

We show that a mixed mode of dislocations is nucleated and emitted from kink-step. Hard mode I dislocation travels in the direction inclined to the TB; therefore, it tends to be impinged by the TB plane. Adding extra parallel TBs into the NW unambiguously obstructs the transmission of hard mode I dislocations. Confined twin spacings in defective NWs have been revealed to attain low yield strength and a strain-hardening effect due to dislocation pinning. The mechanism of dislocation pinning of hard mode I dislocation can be revealed through dislocation reaction. Besides, hard mode II dislocation could also react with kink-steps during its transmission. The mechanisms of dislocation pinning with kink-steps between dislocation modes can also be evaluated via dislocation reaction.

Atomic trajectories in Figure 9 capture the strengthening phenomenon from the additional defective TB layer. Since very limited room is found between TBs, dislocation pinning with kink-steps takes place readily in the NW. Depending on the type of dislocation, dislocation pinning is categorised into two types, as shown in Figure 9 (a) and (b). Dislocations from the kink-steps are often constrained by neighbouring kink-steps. The dislocation scarcely moves and the pinning effect can only be removed with further straining. By invoking double Thompson tetrahedron in TB interface [29], hard mode I dislocation DA from kink-step firstly dissociate into partial dislocation $D\gamma$ and γA. The reaction of hard mode I dislocation pinning is achieved via:

$$DA \rightarrow D\gamma + \gamma A \tag{7}$$

$$D\gamma + \gamma A + A\delta \rightarrow D\gamma + \gamma\delta \tag{8}$$

Another type of dislocation pinning occurs in the course of the transmission of hard mode II dislocation. The slip systems usually sustain maximum Schmid factor and the slip direction is parallel to the TB growth direction. When hard mode II dislocation slides within the NW, it is likely to react with ITB segments to account for dislocation pinning. The kink-step comprises of three partial dislocation *b2:b1:b3*, Hence, this reaction, which is akin to the pinning reaction in [14], is completed by

$$AC \rightarrow A\beta + \beta C \tag{9}$$

$$A\beta + \beta C + C\delta \rightarrow A\beta + \beta\delta \tag{10}$$

The incoming dislocation (*AC*) reacts with the kink-step (*Cδ*). It is noted that a partial dislocation (*Aβ*) and a stair-rod dislocation (*βδ*) or Lomer-Cottrell joint forms, respectively. A Lomer-Cottrell joint can be also generated as the product of the intersection of sliding dislocations. That joint impedes the transmission of dislocation, which is expected to be destroyed with further straining. Here, kink motion is readily activated in the dislocation-intensive regions. The kink on the middle TB layer is reduced from 6-atom-layer-height to 3-atom-layer-height as dissociation of ITB segments. The 3-layered kink-step is seen to migrate away from its original position. As such, kink migration contributes to TB migration, thereby causing detwinning.

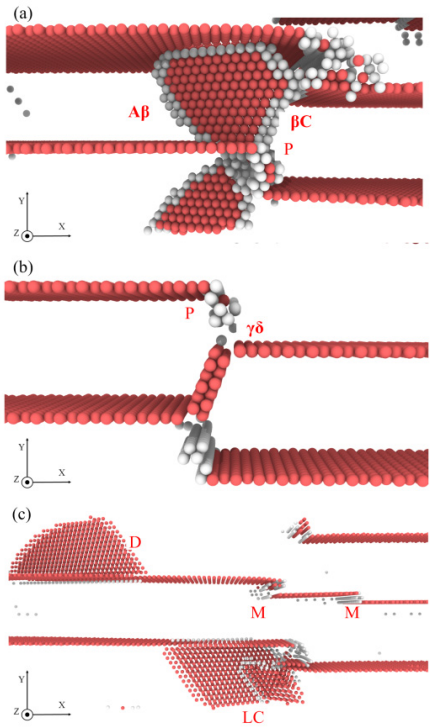

Figure 9. Microstructure of the NW with λ = 3.1 nm. (a) Hard mode II dislocation pinning at ε = 7.0% (b) Hard mode I dislocation pinning at ε = 3.1%. (c) Dislocation/kink events. P represents dislocation pinning, LC represents Lomer-Cottrell dislocation, D represents partial dislocation emitted, M represents kink migration. Perfect Cu atoms and surface atoms are removed to provide a better view of the local GB/dislocation activities.

5. Conclusion

Molecular dynamic simulations were employed to investigate the deformation mechanism of defectively parallel-twinned NWs with respect to yielding and plasticity. The results showed that the presence of kink-steps substantially undermines the strength and enhances the ductility of parallel-twinned NW. A kink-step was found to be more effectual than surface atoms in serving as the source for dislocation nucleation. Two modes of dislocation were initiated from kink-steps and surface atoms, respectively. This study also suggested that the primary plastic mechanisms of a longitudinally deformed NW were kink migration and twin partial multiplication. The kink-steps could dissociate into several segments of kink-step, and the micro-steps moved along the TB plane.

Three key features of kink-steps widely present in the defective NWs were further taken into account, including kink-step density, kink-step height and TB spacing. A critical kink density (one kink/ 4.4nm) was identified where no surface atoms generated dislocation embryos until all kink-steps had served as sites for dislocation emission. Short kink-steps migrated readily, due to the high dislocation force provided to slide, while the kink migration became energy-hungry for larger steps. Unlike perfect NWs, confined defective NWs could result in higher peak strength under the deformation parallel to twin plane. We postulate that the strengthening effect is attributed to constrain hard mode I dislocation by the confined TB spacing. Furthermore, interplay of partial dislocation and TB was observed in the progress of deformation, leaving stair-rod dislocation formed on the twin plane. This reaction could destroy the kink-steps at a high strain. These findings should be incorporated into future analytical consideration of twin boundary structures.

Acknowledgments

This research was undertaken with the assistance of resources from the National Computational Infrastructure (NCI), which is supported by the Australian Government. This work was supported by the Australian Research Council under Grant Nos. LP130101001.

Conflict of Interest

The authors declared that they have no conflicts of interest to this work. We declare that we do not have any commercial or associative interest that represents a conflict of interest in connection with the work submitted.

References

1. Beyerlein IJ, Zhang X, Misra A (2014) Growth twins and deformation twins in metals. *Annu Rev Materi Res* 44: 329–363.
2. Lu L, Shen Y, Chen X, et al. (2004) Ultrahigh strength and high electrical conductivity in copper. *Science* 304: 422–426.
3. Lu L, Chen X, Huang X, et al. (2009) Revealing the maximum strength in nanotwinned copper. *Science* 323: 607–610.
4. Xing B, Yan S, Jiang W, et al. (2016) Atomistic study for the vibrational properties on Σ5 symmetric tilt bicrystal copper nanowires. *Appl Mech Mater* 846: 193–198.

5. Bufford D, Liu Y, Wang J, et al. (2014) In situ nanoindentation study on plasticity and work hardening in aluminium with incoherent twin boundaries. *Nat Commun* 5.
6. Zhang Y, Huang H (2009) Do Twin Boundaries Always Strengthen Metal Nanowires? *Nanoscale Res Lett* 4: 34–38.
7. Zhang J, Yan Y, Liu X, et al. (2014) Influence of coherent twin boundaries on three-point bending of gold nanowires. *J Phys D Appl Phys* 47: 195301.
8. Bezares J, Jiao S, Liu Y, et al. (2012) Indentation of nanotwinned fcc metals: Implications for nanotwin stability. *Acta Mater* 60: 4623–4635.
9. Sun J, Fang L, Ma A, et al. (2015) The fracture behavior of twinned Cu nanowires: A molecular dynamics simulation. *Mater Sci Eng A* 634: 86–90.
10. Kulkarni Y, Asaro RJ, Farkas D (2009) Are nanotwinned structures in fcc metals optimal for strength, ductility and grain stability? *Scripta Mater* 60: 532–535.
11. Gao Y, Sun Y, Yang Y, et al. (2015) Twin boundary spacing-dependent deformation behaviours of twinned silver nanowires. *Mol Simulat* 1–7.
12. Luo Y, Wang Y, Wang Y, et al. (2009) Intrinsic Strengthening of Coherent Twin Boundaries in Copper. *J Mater Sci Technol* 25: 211.
13. Jang D, Li X, Gao H, et al. (2012) Deformation mechanisms in nanotwinned metal nanopillars. *Nat Nanotechnol* 7: 594–601.
14. Cao AJ, Wei YG, Mao SX (2007) Deformation mechanisms of face-centered-cubic metal nanowires with twin boundaries. *Appl Phys Lett* 90: 151909.
15. Wang YM, Sansoz F, LaGrange T, et al. (2013) Defective twin boundaries in nanotwinned metals. *Nat Mater* 12: 697–702.
16. Shute C, Myers B, Xie S, et al. (2011) Detwinning, damage and crack initiation during cyclic loading of Cu samples containing aligned nanotwins. *Acta Mater* 59: 4569–4577.
17. Wang J, Misra A, Hirth J (2011) Shear response of Σ 3 {112} twin boundaries in face-centered-cubic metals. *Phys Rev B* 83: 064106.
18. Fang Q, Sansoz F (2017) Influence of intrinsic kink-like defects on screw dislocation – coherent twin boundary interactions in copper. *Acta Mater* 123: 383–393.
19. Marquis E, Medlin D (2005) Structural duality of 1/3⟨111⟩ twin-boundary disconnections. *Phil Mag Lett* 85: 387–394.
20. Brown J, Ghoniem N (2009) Structure and motion of junctions between coherent and incoherent twin boundaries in copper. *Acta Mater* 57: 4454–4462.
21. Plimpton S (1995) Fast Parallel Algorithms for Short-Range Molecular Dynamics. *J Comp Phys* 117: 1–19.
22. Mishin Y, Mehl MJ, Papaconstantopoulos DA, et al. (2001) Structural stability and lattice defects in copper:Ab initio, tight-binding, and embedded-atom calculations. *Phys Rev B* 63.
23. Wen Y-H, Zhu Z-Z, Zhu R-Z (2008) Molecular dynamics study of the mechanical behavior of nickel nanowire: Strain rate effects. *Comput Mater Sci* 41: 553–560.
24. Stukowski A (2010) Visualization and analysis of atomistic simulation data with OVITO - the Open Visualization Tool *Modelling Simul Mater Sci Eng* 18.
25. Faken D, Jónsson H (1994) Systematic analysis of local atomic structure combined with 3D computer graphics. *Comput Mate Sci* 2: 279–286.
26. Wang J, Li N, Anderoglu O, et al. (2010) Detwinning mechanisms for growth twins in face-centered cubic metals. *Acta Mater* 58: 2262–2270.

27. Li L, An X, Imrich P, et al. (2013) Microcompression and cyclic deformation behaviors of coaxial copper bicrystals with a single twin boundary. *Scripta Mater* 69: 199–202.
28. Zhu T, Gao H (2012) Plastic deformation mechanism in nanotwinned metals: an insight from molecular dynamics and mechanistic modeling. *Scripta Mater* 66: 843–848.
29. Zhu Y, Wu X, Liao X, et al. (2011) Dislocation–twin interactions in nanocrystalline fcc metals. *Acta Mater* 59: 812–821.
30. Li N, Wang J, Misra A, et al. (2011) Twinning dislocation multiplication at a coherent twin boundary. *Acta Mater* 59: 5989–5996.
31. Li X, Wei Y, Lu L, et al. (2010) Dislocation nucleation governed softening and maximum strength in nano-twinned metals. *Nature* 464: 877–880.
32. Xu L, Xu D, Tu KN, et al. (2008) Structure and migration of (112) step on (111) twin boundaries in nanocrystalline copper. *J Appl Phys* 104: 113717.
33. Weertman J (1996) Dislocation based fracture mechanics: World Scientific.

AIMS Press